Approaching Periodic Systems in Ensemble Density Functional Theory *via* Finite One-Dimensional Models

Remi J. Leano,[1] Aurora Pribram-Jones,[1] and David A. Strubbe[2]
[1)] *Department of Chemistry and Biochemistry, University of California, Merced*
[2)] *Department of Physics, University of California, Merced*

(*Electronic mail: dstrubbe@ucmerced.edu)

(*Electronic mail: apj@ucmerced.edu)

(Dated: March 2, 2024)

Ensemble Density Functional Theory (EDFT) is a generalization of ground-state Density Functional Theory (GS DFT), which is based on an exact formal theory of finite collections of a system's ground and excited states. EDFT in various forms has been shown to improve the accuracy of calculated energy level differences in isolated model systems, atoms, and molecules, but it is not yet clear how EDFT could be used to calculate band gaps for periodic systems. We extend the application of EDFT toward periodic systems by estimating the thermodynamic limit with increasingly large finite one-dimensional "particle in a box" systems, which approach the uniform electron gas (UEG). Using ensemble-generalized Hartree and Local Spin Density Approximation (LSDA) exchange-correlation functionals, we find that corrections go to zero in the infinite limit, as expected for a metallic system. However, there is a correction to the effective mass, with results from tri-ensembles similar to literature on 2D and 3D UEGs, indicating promise for non-trivial results from EDFT on periodic systems. Singlet excitation energies are found to be positive, but triplet excitation energies are sometimes negative (a triplet instability), pointing to deficiencies of the approximations.

I. INTRODUCTION

A well known difficulty with ground-state (GS) Density Functional Theory (DFT) is the band gap problem, where the difference between the highest occupied and lowest unoccupied Kohn-Sham (KS) energy states is smaller than the true band gap.[1,2] There are several methods used to extend GS DFT to excited states, including time-dependent DFT (TDDFT)[3–5] and the ΔSCF method.[6–8] TDDFT has become the standard method for calculating the excitation energies of molecules, achieving accuracies comparable to quantities in GS DFT.[9–12] However, in its typical application within the adiabatic approximation, TDDFT inadequately describes double and multiple excitations,[13] and struggles with periodic systems. Typical approximations to the exchange-correlation (XC) kernel f_{xc} lack the correct long-range behavior, which indeed goes goes to zero in the local-density approximation (LDA).[4,5,14–18] Similarly, the correction to excitation energies provided by the ΔSCF method for standard XC approximations goes to zero in periodic systems,[19,20] which some methods have been proposed to solve.[21] The theory of ensemble DFT (EDFT) is another DFT approach to excited states which could be promising for periodic systems, but it remains to be seen how the theory as formulated by Gross, Oliveira, and Kohn[22] can be properly formulated for such systems.

Like GS DFT, EDFT is based on a variational theorem. The difference in the two theories is that while in GS DFT, the GS energy is a functional of the GS density, in EDFT, the ensemble energy is a functional of both the ensemble density and a set of ensemble weights, providing access to excited-state quantities.[22–24] Excitation energies can, in theory, be extracted from the total ensemble energy, and EDFT can account for the discontinuous nature of the XC potential through explicit dependence on weights.[1,25–27] Thus EDFT offers a non-perturbative alternative to TDDFT which can more easily treat multiple- and charge-transfer excitations. Additionally, EDFT can treat both the fundamental (charged)[26] and optical (neutral)[22] gaps of systems. Relatively accurate EDFT calculations have been performed for small atoms,[28,29] the hydrogen molecule,[30] for two electrons in boxes or in a 3D harmonic well (Hooke's atom),[31] the asymmetric Hubbard dimer,[25,32,33] and for some molecules.[34,35] However, developing the necessary weight-dependent functionals in order to use EDFT is a complicated task that remains at an early stage of development and limits EDFT's application to a wider span of systems.[36–44] The key difficulty of EDFT for periodic systems is that the excited states of solids are a continuum of states and as such cannot be modelled with existing EDFT approaches which construct the ensemble from a finite number of individual states.[22]

In this paper, rather than studying a periodic system in EDFT directly, we study EDFT by means of finite one-dimensional (1D) systems approaching the thermodynamic limit, performing DFT calculations in the open-source real-space code Octopus.[45,46] In section II A we introduce a 1D system whose KS potential is a "particle in a box" (PIB). We build ensembles for the system with the weighting scheme described in section II B. We motivate our choice of weight-dependent functionals in section II C and describe the multiplet structure and construction of many-electron densities for our system in section II D. In sections II E and II F we outline the necessity of studying systems in the approach to the thermodynamic limit rather than direct study of periodic systems within EDFT. In section III, we describe our computational methodology for calculations of first (triplet) and second (singlet) excitation energies. Finally, in section IV, we discuss ensemble corrections to excitation energies, a triplet instability found from the bi-ensemble, and effective masses obtained in the approach to the thermodynamic limit. We find non-trivial renormalization of the effective masses with results from the

tri-ensemble similar to the uniform electron gas in other dimensionalities, showing the promise of EDFT for describing periodic systems.

II. THEORY

A. The 1D PIB Potential is the KS Potential

The PIB potential is defined as a free particle within the confines of a box of length $2L$, subject to an infinite potential outside these boundaries:

$$V(x) = \begin{cases} 0, & -L < x < L, \\ \infty, & x \leq -L \text{ or } x \geq L. \end{cases} \tag{1}$$

The PIB is more readily adaptable to study in the thermodynamic limit than atom-based models, and in the limit it becomes the uniform electron gas (UEG) which is a prototypical model in electronic structure theory and is used as a simplified model for the behavior of electrons in metals.[47] The 1D UEG is known from the Lieb-Mattis theorem[48] to be a singlet at all densities, which has also been found in quantum Monte Carlo calculations.[49] It is also expected to be metallic according to Luttinger liquid theory.[50,51] In this work, we set the KS potential, v_{KS}, equal to the PIB potential such that $v_{\mathrm{KS}}(r) = 0$ within the boundaries of the box. Setting v_{KS} rather than v_{ext} to the PIB potential allows us to determine the KS wavefunctions and eigenvalues exactly, and bypasses the need to solve for them self-consistently. A similar approach has been used in studies of a model atom whose KS potential is $1/r$.[52] In the thermodynamic limit, we obtain the UEG, whether we set v_{ext} or v_{KS} equal to the PIB potential. In this limit, the density is constant, leading to a constant $v_{\mathrm{Hxc}}[\rho]$, which provides only an overall offset to the eigenvalues and no difference in the excitation energies.

Here we first discuss such a set-up in the context of GS DFT, and then describe the construction of the ensemble in section II B. In GS-DFT, the KS potential is defined as

$$v_{\mathrm{KS}}(r) = v_{\mathrm{ext}}(r) + e^2 \int \frac{\rho(r')}{|r-r'|} dx' + \frac{\delta E_{\mathrm{xc}}[\rho(r)]}{\delta \rho(r)}, \tag{2}$$

where $r = \{x, \omega\}$ indicates both space and spin coordinates. For simplicity, we limit our study to 1D, though a similar procedure could be followed for 2D or 3D. Here the first term on the right is the external potential, the second term is the Hartree potential (where e is the electron charge), and the third term is the XC potential. The KS equations are:

$$\left\{ -\frac{\hbar^2}{2m}\nabla^2 + v_{\mathrm{KS}}(r) \right\} \varphi_j(r) = \varepsilon_j \varphi_j(r), \tag{3}$$

where the set of spin-polarized wavefunctions $\{\varphi_j\}_{1 \leq j \leq \infty}$ are the lowest-energy solutions. The KS many-body wavefunction Ψ, generally assumed to be a single Slater determinant, is built from $\{\varphi_j\}$. Both $\{\varphi_j\}$ and their corresponding energies $\{\varepsilon_j\}_{1 \leq j \leq \infty}$ are typically obtained iteratively from SCF calculations, but in this case, because we have set $v_{\mathrm{KS}}(r) = 0$, we know ε_j exactly from the analytical solutions to the non-interacting PIB problem:

$$\varepsilon_n = \frac{n^2 \pi^2 \hbar^2}{8 m_e L^2}, \tag{4}$$

where m_e is the mass of an electron. For the same reason, we know the wavefunctions solving equation (3) exactly, which are defined by their quantum number n:

$$\phi_n(x) = \sqrt{\frac{1}{L}} \sin\left(\frac{n\pi}{2L} x\right), \qquad (n = 1, 2, ...). \tag{5}$$

From each spatial wavefunction, $\phi(x)$, one can form two different orthonormal spin and space-dependent wavefunctions by multiplying the spatial function by the up $\alpha(\omega)$ or down $\beta(\omega)$ spin function:[53]

$$\varphi(r) = \begin{cases} \phi(x)\alpha(\omega) \\ \quad \text{or} \\ \phi(x)\beta(\omega), \end{cases} \tag{6}$$

The density for a system of non-interacting particles is:

$$\rho(r) = \sum_{j=1}^{\infty} f_j |\varphi_j(r)|^2, \tag{7}$$

with occupations $f_j \in \{0, 1\}$ to specify occupied and unoccupied states. Up to two φ_j may correspond to the same ϕ_n, which is the case for a doubly occupied spatial state. Knowing the non-interacting density, the sum of the wavefunction energies, the Hartree energy and an approximation to the XC energy functional, the total interacting energy is obtained as[47]

$$E^{\mathrm{tot}}[\rho(r)] = \sum_j^{\infty} f_j \varepsilon_j - E_H[\rho(r)] - \int (v_{\mathrm{xc}}(\rho; r))\rho(r) dx + E_{\mathrm{xc}}[\rho(r)], \tag{8}$$

where $\frac{\delta E_{\mathrm{xc}}[\rho(r)]}{\delta \rho(r)} = v_{\mathrm{xc}}$. Equation (8) is exact if the XC functional is known exactly.

B. Ensemble Density Functional Theory

EDFT as discussed here stems from Theophilou and Gidopoulos's work in 1987 which built ensembles from KS states.[54] This variational principle for equi-ensembles was generalized to ensembles of monotonically decreasing, non-equal weights by Gross-Oliveira-Kohn (GOK) in 1988.[22] To avoid confusion, we note that the theory of thermal "Mermin" DFT,[55] commonly used for periodic systems such as metals, has been referred to as "ensemble DFT" also,[56] but it is based on a Fermi-Dirac thermal ensemble and thus is quite different from GOK EDFT.

The ensemble-generalized form of equation (3) is the non-interacting ensemble KS equation:

$$\left\{ -\frac{1}{2}\nabla^2 + v_{\mathrm{KS}}^w[\rho^w](r) \right\} \varphi_j^w(r) = \varepsilon_j^w \varphi_j^w(r), \tag{9}$$

where φ_j^w are the non-interacting single-particle wavefunctions that reproduce the ensemble density, $\rho^w(r)$. The KS many-body wavefunctions $\{\Psi_m^w[\rho]\}_{0\le m\le M_I-1}$, assumed to be Slater determinants or linear combinations of Slater determinants, are built from $\{\varphi_j(r)\}_{1\le j\le\infty}$ having individual energies ε_j which are obtained from the ensemble KS equation, equation (9). Symmetry-adapted linear combinations of Slater determinants may be used, as the conventional restriction to single Slater determinants has been found to be overly restrictive in EDFT.[57] The ensemble-generalized form of equation (2) is:

$$v_{\mathrm{KS}}^w[\rho^w](r) = v_{\mathrm{ext}}(r) + \frac{\delta E_{\mathrm{Hxc}}^w[\rho^w]}{\delta\rho^w(r)}, \tag{10}$$

and the ensemble functional for Hartree, exchange, and correlation (HXC), E_{Hxc}^w, may be separated into its constituent parts:

$$\frac{\delta E_{\mathrm{Hxc}}^w[\rho^w]}{\delta\rho^w(r)} = \int\frac{\rho^w(r')}{|r-r'|}dr' + \frac{\delta E_{\mathrm{x}}^w[\rho^w]}{\delta\rho^w(r)} + \frac{\delta E_{\mathrm{c}}^w[\rho^w]}{\delta\rho^w(r)}. \tag{11}$$

While the single-particle wavefunctions $\{\varphi_j^w\}$ and their corresponding energies $\{\varepsilon_j\}$ are calculated in the same way as in the GS case presented in section II A, the ensemble density is constructed in a different way than the GS equation (7):

$$\rho^w(r) = \sum_{m=0}^{M_I-1}\mathtt{w}_m\left(\sum_{j=1}^{\infty}f_j^m|\varphi_j(r)|^2\right), \tag{12}$$

where f_j^m denotes the occupation of $\varphi_j(r)$ in the mth KS wave function $\Psi_m^w[\rho^w]$.[41] I denotes the set of degenerate states (or "multiplet") with the highest energy in the ensemble. This set can be equivalently referred to as the (M_I-1)th state, as we consider an ensemble of M_I (possibly degenerate) electronic states each consisting of N_e electrons, numbered from $m=0$ to M_I-1. Then, g_I is the multiplicity of the Ith multiplet, and M_I is the total number of states up to and including the Ith multiplet, $M_I=\sum_{j=0}^{I}g_j$.[22,41] $I=1$ denotes a bi-ensemble, and $I=2$ denotes a tri-ensemble, as depicted in figure 1.

GOK ensembles must include all of each degenerate subspace to be well-defined. Each many-electron state's energy is denoted by $E_{m=0}\le\ldots\le E_{m=M_I-1}$, and the energy of the mth KS state is

$$E_m = \sum_{j=1}^{\infty}f_j^m\varepsilon_j, \tag{13}$$

which can be obtained exactly in this case from equation (4). Each state is assigned a weight $\mathtt{w}_m$ from the set $\{w\}\equiv(\mathtt{w}_{m=0},\ldots,\mathtt{w}_{m=M_I-1})$ of monotonically non-increasing $(\mathtt{w}_{m=0}\ge\ldots\ge\mathtt{w}_{m=M_I-1})$ weights obeying

$$\sum_{m=0}^{M_I-1}\mathtt{w}_m = 1. \tag{14}$$

For the GOK-I ensembles considered here, the weights are defined as[22]

$$\mathtt{w}_m = \begin{cases}\frac{1-\mathtt{w}g_I}{M_I-g_I} & m<M_I-g_I,\\ \mathtt{w} & m\ge M_I-g_I,\end{cases} \tag{15}$$

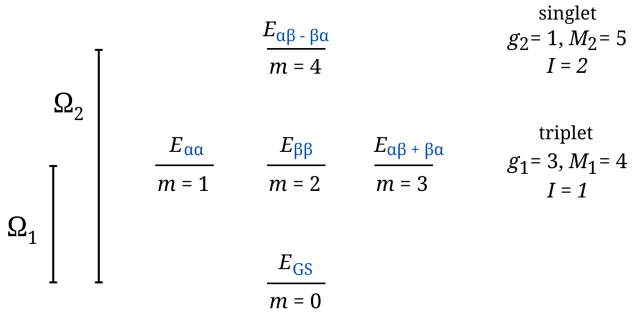

Figure 1. Diagram of the multiplet structure for the ensemble of interacting particles for a PIB, obeying spin symmetry. $I=1$ corresponds to the bi-ensemble, which includes up to $m=3$ (1st multiplet). $I=2$ corresponds to the tri-ensemble, which includes up to $m=4$ (2nd multiplet). The degeneracy of the highest multiplet included in the ensemble is given by the corresponding value of g_I, and M_I is the total number of states included in the Ith ensemble. The assignment of m's within a multiplet are arbitrary.

where $\mathtt{w}\in[0,1/M_I]$, such that all states but those in the highest (Ith) multiplet have the same weight, and only the GOK weight, $\mathtt{w}$, is needed to define the weighting of the ensemble. By definition, $\mathtt{w}=\mathtt{w}_{M_I-1}$. The total ensemble energy is[22]

$$\begin{aligned}\mathscr{E}^w[\rho^w(x)] &= \sum_{m=0}^{M_I-1}E_m - E_{\mathrm{H}}[\rho^w(r)]\\ &-\int\left(v_{\mathrm{XC},\alpha}(\rho_\alpha^w;r)\right)\rho_\alpha^w(r)d^3r - \int\left(v_{\mathrm{XC},\beta}(\rho_\beta^w;r)\right)\rho_\beta^w(r)d^3r\\ &+E_{\mathrm{x}}^{\mathrm{LDA}}[\rho^w(r)] + E_{\mathrm{c}}^{\mathrm{LDA}}[\rho^w(r)].\end{aligned} \tag{16}$$

The exact ensemble energy is obtained if the ensemble HXC functional is known exactly.

By differentiating equation (16) with respect to $\mathtt{w}$, one obtains the excitation energy Ω_I of multiplet I from the GS:[33]

$$\Omega_I = E_I - E_0 + \left.\frac{\partial E_{\mathrm{Hxc}}^w[\rho]}{\partial\mathtt{w}}\right|_{\rho=\rho^w}. \tag{17}$$

The third term on the right of equation (17) is the "ensemble correction" to the non-interacting difference of energies between the Ith KS state and the GS from equation (13), E_I–E_0.

C. Approximations to Hartree, Exchange, and Correlation

The development of accurate weight-dependent density-functional approximations (DFAs) for EDFT is an ongoing challenge. Existing ensemble approximations to E_{xc}^w include the quasi-local-density approximation (qLDA) functional,[36,37] the "ghost"-corrected exact exchange (EXX) functional,[38,39] the exact ensemble exchange functional (EEXX),[40] a local system-dependent and excitation-specific ensemble exchange functional for double-excitations (CC-S),[41] a universal weight-dependent local correlation functional (eVWN5) based on finite UEGs,[41] and the orbital-dependent second-order perturbative approximation (PT2) for

the ensemble correlation energy functional.[42] As noted in all the aforementioned works, ensemble HXC has special complications beyond those of GS DFT, such as the consideration that ensemble Hartree and exchange are not naturally separated in EDFT.[43] Though each of these approaches above to approximating ensemble XC energies provides insight into the necessary characteristics of ensemble DFAs, it is unclear whether any of them are appropriate for periodic systems since they were developed for localized systems. In this work, for a first exploration of EDFT on periodic systems, we choose a simple approximation based on a Local Spin Density Approximation (LSDA).

The "traditional" DFAs of GS DFT can be used for ensembles by evaluating them on ensemble densities:

$$E_{\mathrm{Hxc}}^{\mathrm{trad}}[\rho] = E_{\mathrm{Hxc}}\left[\sum_{m=0}^{M_I-1} \mathtt{w}_m \rho_m(r)\right]. \tag{18}$$

This use of the ensemble density with GS DFAs, typically only applied to Hartree and exchange, has been called "*Ansatz* 1."[43] The use of ensemble densities in "traditional" GS DFAs results in fictitious interactions of ground- and excited-state densities, or "ghost interaction errors" (GIEs), in both Hartree and exchange which do not cancel each other.[31,36,39,43,58] Additionally, with this form of ensemble DFA, the derivatives in equation (17) become zero, since the weight dependence is within the ensemble density only. As such, nothing is learned from application of EDFT in such an approximation. We instead opt to use ensemble-generalized LSDA, in which we build an ensemble average by evaluating the GS Hartree and LSDA functionals on the density of each state in the ensemble individually:

$$E_{\mathrm{Hxc},w}^{\mathrm{LSDA}}[\rho] = \sum_{m=0}^{M_I-1} \mathtt{w}_m E_{\mathrm{Hxc}}^{\mathrm{LSDA}}[\rho_m(r)], \tag{19}$$

which has been called "*Ansatz* 2."[43] In this way, we ensure the ensemble functionals to be weight-dependent, giving us nonzero corrections in equation (17).

Derivatives of this equation with respect to $\mathtt{w}$ depend on the weights defined in equation (15), which in turn are determined by the multiplet structure and I, e.g., whether a bi-ensemble or tri-ensemble is used (figure 1), and have the general form:

$$\left.\frac{\partial E_{\mathrm{Hxc}}^{\mathrm{LSDA},w}[\rho]}{\partial \mathtt{w}}\right|_{\rho=\rho^w} = -\frac{g_I}{M_I-g_I}\sum_{m=0}^{M_I-g_I-1} E_{\mathrm{Hxc}}[\rho_m(r)] + \sum_{m=M_I-g_I}^{M_I-1} E_{\mathrm{Hxc}}[\rho_m(r)]. \tag{20}$$

Note a useful property: the sum of the coefficients of the M_I states is

$$-\frac{g_I}{M_I-g_I}(M_I-g_I)+(1)\,g_I = 1-1 = 0. \tag{21}$$

This property is essential allow the excitation energy be intensive (size-consistent) as we approach the thermodynamic limit, since individual total energy terms are extensive and grow without bound. We note that the form of equation 20 neglects any implicit weight-dependence of the densities from the fact that the derivative should be taken at constant density.

This definition of ensemble-generalized Hartree is GIE-free.[31] Though this choice avoids a significant source of GIE, our current form of ensemble-generalized LSDA does introduce some GIE from XC.[43] We report results for ensemble corrections which have been built using the weight-dependent Hartree of equation (19), denoted by HXC, and also for the case where there is no Hartree contribution to the correction, denoted by XC, due to the "traditional" Hartree definition in equation (18).

D. Densities of Ground and Excited States

Here we show explicitly the spin-polarized densities involved in the ground and excited states which we use in our EDFT calculations. All densities involved here include a contribution from the closed shell,

$$\rho_{\mathrm{closed}}(r) = \sum_{n=1}^{N_e/2-1} |\phi_n(r)|^2\left(|\alpha(\omega)|^2+|\beta(\omega)|^2\right), \tag{22}$$

and the ground-state density is

$$\rho_{\mathrm{GS}}(r) = |\phi_1(x)|\left(|\alpha(\omega)|^2+|\beta(\omega)|^2\right)+\rho_{\mathrm{closed}}(r), \tag{23}$$

where ϕ_1 is the highest occupied state.

In the spin-polarized PIB system of even N_e, based on spin symmetry, the system has a nondegenerate GS, a triplet first excited state, and a singlet second excited state, as depicted in figure 1. An odd number of N_e would result in a different multiplet structure, but we do not investigate that case here, since odd/even distinctions should disappear in the thermodynamic limit anyway. The density of the $\alpha\alpha$ state ($m_s = 1$) in the triplet, obtained from its Slater determinant and then written in terms of its constituent wavefunctions, is:

$$\rho_{\alpha\alpha}(r) = |\phi_1(x)\alpha(\omega)|^2+|\phi_2(x)\alpha(\omega)|^2+\rho_{\mathrm{closed}}(r), \tag{24}$$

where ϕ_2 is the lowest unoccupied state, with reference to the ground state. Then, for the $\beta\beta$ ($m_s = -1$) state in the triplet, we obtain a similar equation where the α spins are flipped to β spins:

$$\rho_{\beta\beta}(r) = |\phi_1(x)\beta(\omega)|^2+|\phi_2(x)\beta(\omega)|^2+\rho_{\mathrm{closed}}(r). \tag{25}$$

While $\rho_{\alpha\alpha}(r) \neq \rho_{\beta\beta}(r)$, our approximations to the energy-density functional, evaluated on these two densities, yields the same numerical result for their energies as required by symmetry, and is the result obtained from any LSDA. For the $m_s = 0$ excited states, we must use linear combinations of two Slater determinants to obtain the density:

$$\rho_{\alpha\beta\pm\beta\alpha}(r) = \frac{1}{2}\Big(|\phi_1(x)\alpha(\omega)|^2+|\phi_1(x)\beta(\omega)|^2+ |\phi_2(x)\alpha(\omega)|^2+|\phi_2(x)\beta(\omega)|^2\Big)+\rho_{\mathrm{closed}}(r). \tag{26}$$

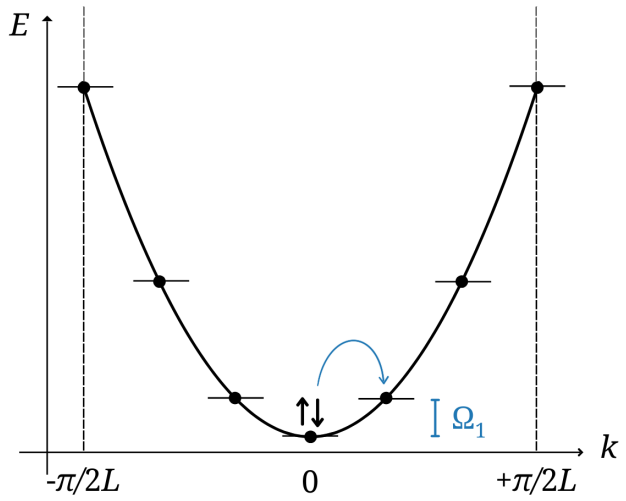

Figure 2. Band structure of the free electron gas, shown with a discrete set of 6 k-points in a Brillouin zone based on a periodic length $2L$. Arrow depicts an excitation with $\Delta k > 0$.

We obtain the same density for the symmetric triplet $(+)$ and antisymmetric singlet $(-)$ sum of the two Slater determinants. No pure density functional can tell the two states, having identical densities, apart, despite the fact that the triplet should be degenerate with the other two triplet states.

We will consider later, in sections III C and III D, two approaches to treating the triplet energy. The first method, outlined in III D, is the symmetry-broken tri-ensemble, in which the correct densities for each state in the triplet, obtained from equations (24), (25), and (26), are used. Although $E_{\rm xc}[\rho_{\alpha\alpha}]$ and $E_{\rm xc}[\rho_{\beta\beta}]$ are equal, the energy $E_{\rm xc}[\rho_{\alpha\beta+\beta\alpha}]$ of the third member of the triplet has a higher energy, with their difference decreasing asymptotically towards 0 as $N_e \to \infty$. To address this issue, we have also considered the symmetry-enforced tri-ensemble in section III C, in which we do not use the computed value of $E[\rho_{\alpha\beta+\beta\alpha}]$ at all, and instead use the value of $E[\rho_{\alpha\alpha}] = E[\rho_{\beta\beta}]$ to represent all three states, maintaining the degeneracy of the KS states forming the spin triplet. Since both the singlet and triplet ($m_s = 0$) states have the same density, we write $\rho_{\alpha\beta\pm\beta\alpha}$ in sections II E, III C, and III D to refer to their shared density.

GOK ensemble theory requires that states are ordered based on the energies of the interacting system, and that all states from the GS up to and including the Ith multiplet are included in the ensemble. It is not always practically feasible to be certain that there are no additional states lying between those we have included in the system,[41] but we work under the assumption that we have included all states between the ground state and Ith excited state, such that we have not violated the rules of the GOK ensemble.

E. 1D Uniform Electron Gas

We first consider a possible way that a periodic system, could be discretized to allow application of EDFT. Leaving aside the question of whether such an approach is theoretically sound, we find that in the case of the UEG (the limit of our model) corrections to the KS excitation energies are identically zero, demonstrating that alternate strategies are needed in order to obtain non-trivial results.

We consider an infinite limit of our system in which the KS potential is zero everywhere, and periodic boundary conditions $\phi(x+2L) = \phi(x)$ are imposed for an arbitrary repeating cell of length $2L$. The KS wavefunctions have the form

$$\phi_k(x) = \sqrt{\frac{1}{2L}} e^{ikx}, \tag{27}$$

and the KS energies for such a 1D system are

$$E = \frac{\hbar^2 k^2}{2m_e}, \tag{28}$$

as discussed further in section IV C.

This system has a continuous spectrum of states and, as noted earlier, the GOK EDFT has been defined only for a discrete spectrum. We artificially discretize by choosing a set of k-points such as $k = (n/3)(\pi/2L)$ where $n = \{0, \pm1, \pm2, 3\}$. This discretization is equivalent to construction of a "finite, but topologically periodic system", like a particle on a ring,[59] such as one might construct to avoid the edge effects of our finite PIBs. We consider an excitation with $\Delta k > 0$, to keep things simple and involve only one excited KS energy level – while this bends the rules of the GOK EDFT by not assigning the same weights to all of a degenerate set, it can be justified in a generalization in which states of different symmetry (e.g. crystal momentum k) can be treated separately.[60] With the two KS energy levels, we obtain a singlet-triplet structure which is the same as in our finite well with even N_e (Section II A and figure 1). Filling the system with 2 electrons per cell of $2L$ results in two electrons in the lowest k-point, as in figure 2. With two electrons per unit cell, moving an electron from one k-point to the next represents exciting $1/2$ of all electrons in the periodic system. All of the ground- and excited-state densities are constant; e.g. from equation (24) we obtain:

$$\rho_{\alpha\alpha}(r) = \left|\sqrt{\frac{1}{2L}} e^{ik_1 x}\alpha(\omega)\right|^2 + \left|\sqrt{\frac{1}{2L}} e^{ik_2 x}\alpha(\omega)\right|^2 = \frac{1}{L}, \tag{29}$$

where $k_2 = k_1 + \Delta k$. We find the same result for the three states which make up the triplet of the first excited state, equations (26), (24), and (25), and for the GS. The energy correction, as will be shown in Section III A, is

$$\left.\frac{\partial E^w_{\rm Hxc}[\rho]}{\partial \mathtt{w}}\right|_{\rho=\rho^w} = -3E_{\rm Hxc}[\rho_{\rm GS}] + E_{\rm Hxc}[\rho_{\alpha\alpha}] + E_{\rm Hxc}[\rho_{\beta\beta}] + E_{\rm Hxc}[\rho_{\alpha\beta\pm\beta\alpha}] = 0, \tag{30}$$

where each density is identical, and the total correction goes to zero because the coefficients in front of each energy term

always sum to zero (equation (21)). Since the GOK ensemble correction depends on the ensemble density defined in equation (12), and each state has the same density, it is not possible to obtain a non-zero correction from EDFT to the UEG in this manner. Changing the number of electrons, number of k-points, length of the box, or which excitation we calculate (e.g. including $\Delta k < 0$) would change the complexity for this model, but not the basic conclusion. We instead study a finite system which increases in size towards the thermodynamic limit to gain information about the behavior of EDFT's correction as it approaches a periodic system.

F. Thermodynamic Limit of the Finite-Length Well

We increase the number of electrons in our system along with the length of the box, holding the average density constant:

$$\frac{N_e}{2L} = 0.5 \text{ Å}^{-1} \qquad N_e, L \to \infty. \tag{31}$$

As $N_e \to \infty$, a region of increasingly constant density begins to form at the center of the box, with decreasing oscillations and decreasing edge regions. According to the Wentzel–Kramers–Brillouin (WKB) Approximation, there will always be a peak at the classical turning points,[61] i.e. the edges of the box. As both N_e and L approach infinity, the density of the system becomes more uniform, with the nonuniform edge regions decreasing in width. To quantify this property (figure 3), we first find the height $\rho^{\max}$ of the highest peak within $-L \le x \le 0$. We average the values of the peaks and troughs of the density at the center ($x = 0$) to find the average uniform density ρ^{uniform}. We then define $\Delta\rho^{\max} = \rho^{\max} - \rho^{\text{uniform}}$. Next, we consider an envelope function that excludes the oscillations of the density by linearly connecting the peaks of the density. We determine the width Δx of the region between the edge of the box and the position at which the envelope has decreased to $\Delta\rho^{\max}/e$ measured from ρ^{uniform}. We note that Δx decreases not only as a fraction of L but also in absolute terms, demonstrating that our model becomes increasingly uniform with increasing L and that edge effects become negligible (figure 4). In this way, our model systems in the approach to the thermodynamic limit can be used to study how EDFT performs in a uniform periodic system.

III. COMPUTATIONAL METHODOLOGY

Octopus is uniquely suited for this work due to its ability to define arbitrary potentials and therefore easily treat model systems and 1D systems.[45,46] In this work we use Octopus version 11.4. In order to realize our condition of setting the KS potential equal to the 1D finite well potential in Octopus, the potential is set to zero within a finite domain determined by L. The wavefunction is constrained to zero at the boundaries of the box. We limit our system to an even number of electrons N_e whose ratio to L is held fixed as in equation (31), and

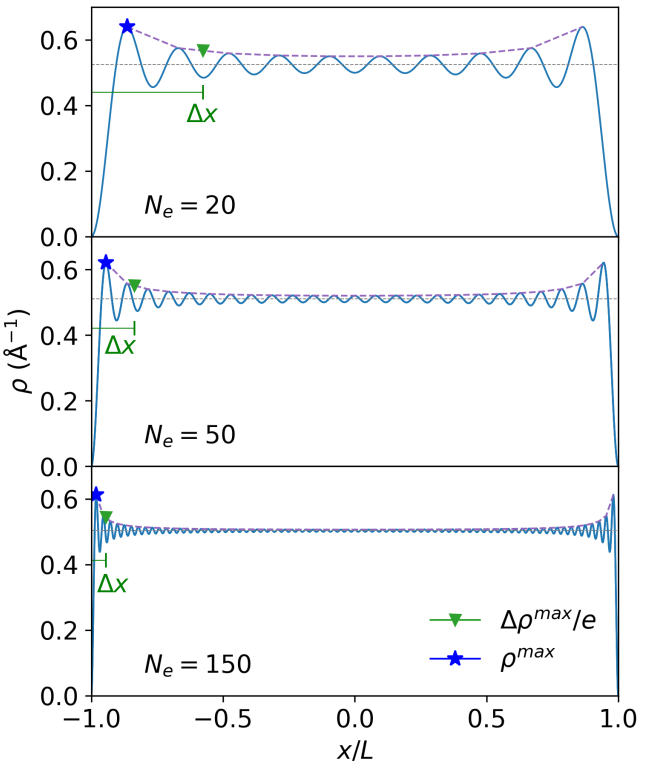

Figure 3. The non-interacting ensemble densities for $N_e = 20$, $N_e = 50$, and $N_e = 150$, with interpolation line (dashed) between peaks. The maximum of the density within $-L \le x \le 0$ is $\rho^{\max}$. The average density at the center of the box is shown as a dotted horizontal line. The width of the edge region, Δx, is defined as the width from the edge of the box to the point at which the interpolation line is $\Delta\rho^{\max}/e$ from the center peak-to-peak amplitude average, as described in section II F. The width of Δx spans a smaller portion of the box as N_e increases.

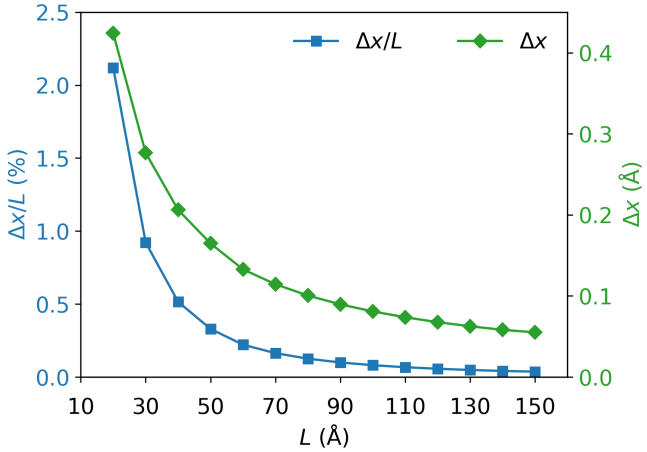

Figure 4. Decreasing width of the edge regions of the density, with increasing L. The average density is held constant to 0.5 Å^{-1} as in equation (31). The right axis is the width of the region Δx, and the left axis is the percentage of the half-length of the box spanned by Δx.

consider its spin-polarized solutions obtained from the PIB as in equations (5) and (7). The starting initial guess in the Kohn-Sham equations are random wavefunctions. We used the conjugate-gradients eigensolver with a tolerance of 10^{-6} eV, which can require up to 1000 eigensolver iterations, and did not use a preconditioner. Eigensolver convergence was difficult to achieve and we settled on this fixed density ratio, grid, and the eigensolver to give adequate convergence behavior. The average density of 0.5 Å^{-1} was used to achieve eigensolver convergence since systems with the larger average density of 1 Å^{-1} were unable to be converged for all values of N_e. A grid spacing of 0.01 Å is used for all calculations in order to converge energy eigenvalues to within 0.05 eV of the analytic solutions of the PIB. Though the KS eigenvalues and eigenfunctions can be obtained analytically, we use the values obtained from Octopus for consistency in comparing to the ensemble-generalized LSDA HXC values which we obtain from Octopus.

For each choice of N_e, we first run a spin-polarized GS calculation for independent particles in 1D, calculating $N_e/2+1$ states to include all the filled states plus one unoccupied state. We then run a "one-shot" DFT calculation with the same value of N_e, but occupations of the KS states for each state in the ensemble are built based on f_j^m of equation (12), which are obtained from Slater determinants as outlined in section II D. These calculations use fixed wavefunctions from the previous independent-particles calculation, and provide E_H, E_x, and E_c for a density built from the given occupations.

Given the problematic nature of the Coulomb interaction in 1D, we describe the electron-electron interactions with the 1D soft Coulomb potential, where we set the softening parameter, a, to 1 Bohr radius (a_0):

$$v_\text{sc}(x) = \frac{1}{\sqrt{x^2+a^2}}. \tag{32}$$

We use the 1D LSDA exchange[62] and correlation functionals[63] as implemented in `libxc` 4.3.4,[64] which were parametrized for this interaction and value of a.

A. Bi-ensemble: Symmetry-enforced

Starting from equation (19), the GOK weighting scheme from equation (15), and the multiplet structure of figure 1A with a choice of the bi-ensemble ($I=1$, $g_1=3$ and $M_1=4$), our weights are:

$$\mathtt{w}_m = \begin{cases} 1-3\mathtt{w} & m<1, \\ \mathtt{w} & m\geq 1. \end{cases} \tag{33}$$

The corresponding excitation energy correction from equation (20), as in equation (30) for the UEG, is

$$\left.\frac{\partial E^w_\text{Hxc}[\rho]}{\partial \mathtt{w}}\right|_{\rho=\rho^w} = -3E_\text{Hxc}[\rho_\text{GS}] + E_\text{Hxc}[\rho_{\alpha\alpha}] + E_\text{Hxc}[\rho_{\beta\beta}] + E_\text{Hxc}[\rho_{\alpha\beta\pm\beta\alpha}]. \tag{34}$$

To use this expression directly would break the spin-symmetry of the triplet, as noted in Section II D. We note that other EDFT methods have avoided this symmetry-breaking issue via approximations based on multi-determinant spin eigenstates rather than just the density.[31] To enforce spin symmetry, we use the energy $E_\text{Hxc}[\rho_{\alpha\alpha}]$ for all states in the triplet, simplifying equation 34 to:

$$\left.\frac{\partial E^w_\text{Hxc}[\rho]}{\partial \mathtt{w}}\right|_{\rho=\rho^w} = -3E_\text{Hxc}[\rho_\text{GS}] + 3E_\text{Hxc}[\rho_{\alpha\alpha}]. \tag{35}$$

Revisiting equation (17), it becomes apparent that the difference of KS energies $E_I - E_0$ can be reduced to a difference of eigenvalues *via* equation (13):

$$E_I - E_0 = \sum_{j=1}^{\infty} f_j^I \varepsilon_j - \sum_{j=1}^{\infty} f_j^0 \varepsilon_j. \tag{36}$$

This expression reduces to the same result for both the bi-ensemble ($I=1$) and, as needed later in sections III C and III D, the tri-ensemble ($I=2$) – that is, $E_2 - E_0 = E_1 - E_0 = \varepsilon_{n=2} - \varepsilon_{n=1}$. To calculate the excitation energy Ω_I of equation (17), we still must calculate the third term, the derivative of the HXC functional with respect to the weight. Combined with equation (36), the first excitation energy from equation (17), denoted Ω_2^e with 'e' for symmetry-enforced approach, is:

$$\Omega_1^\text{e} = \varepsilon_{n=2} - \varepsilon_{n=1} - 3E_\text{Hxc}[\rho_\text{GS}] + 3E_\text{Hxc}[\rho_{\alpha\alpha}]. \tag{37}$$

B. Bi-ensemble: Symmetry-broken

In a second alternative method, we do not enforce any symmetry, and only simplify equation (41) based on equalities that are satisfied in practice by LSDA. We use $E_\text{Hxc}[\rho_{\alpha\alpha}]$ for only two states in the triplet. $E_\text{Hxc}[\rho_{\alpha\beta\pm\beta\alpha}]$ is then used for the third state of the triplet, breaking the spin symmetry. The first excitation energy from equation (17), denoted Ω_2^b with 'b' for symmetry-broken approach, is calculated as:

$$\Omega_1^\text{b} = \varepsilon_{n=2} - \varepsilon_{n=1} - 3E_\text{Hxc}[\rho_\text{GS}] + 2E_\text{Hxc}[\rho_{\alpha\alpha}] + E_\text{Hxc}[\rho_{\alpha\beta\pm\beta\alpha}]. \tag{38}$$

The difference between triplet energies from the symmetry-enforced and symmetry-broken bi-ensembles, from equations (37) and (38) is:

$$\Omega_1^\text{e} - \Omega_1^\text{b} = E_\text{xc}[\rho_{\alpha\alpha}] - E_\text{xc}[\rho_{\alpha\beta\pm\beta\alpha}]. \tag{39}$$

Because the Hartree term is spin-independent, its value is the same when evaluated on $\rho_{\alpha\alpha}$ and $\rho_{\alpha\beta\pm\beta\alpha}$. For this reason, the difference in corrected excitation energies obtained in equation (39) only has a contribution from XC, and is the same whether an ensemble-generalized Hartree is used or not.

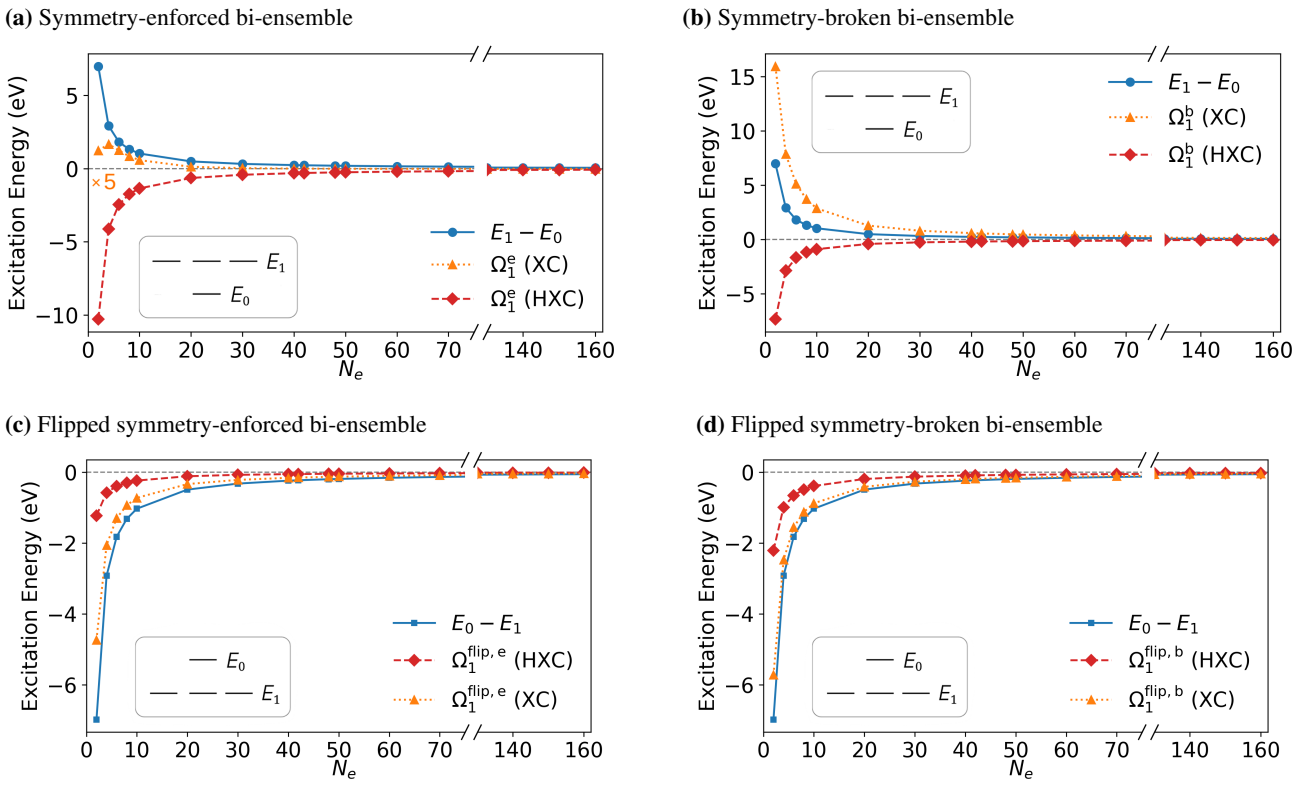

Figure 5. Ensemble-corrected first excitation energies compared to KS energy differences for: **(a)** the triplet Ω_1^{e} of the symmetry-enforced bi-ensemble described in section III A and by equation (37), where Ω_1^{e} (XC) has been scaled up by a factor of 5 for visibility; **(b)** the triplet Ω_1^{b} of the symmetry-broken bi-ensemble described in section III B and by equation (38); **(c)** the singlet $\Omega_1^{\text{flip,e}}$ of the flipped symmetry-enforced bi-ensemble, described in section IV A and by equation (46); and **(d)** the singlet $\Omega_1^{\text{flip,b}}$ of the flipped symmetry-broken bi-ensemble, described in section IV A and by equation (47). Insets show the relative ordering of the first excited state and ground state for each ensemble. The labels 'e' and 'b' denote results from the symmetry-enforced and symmetry-broken ensembles. HXC denotes results with a weight-dependent Hartree, while XC denotes the use of a "traditional" Hartree, as explained in section II C.

C. Tri-ensemble: Symmetry-enforced

We now consider a tri-ensemble, $I = 2$, based on figure 1. In order to calculate the singlet energy, Ω_2, we begin with equation (17). Knowing the difference of non-interacting energies from the PIB, all that is left is to calculate the derivative of E_{Hxc}. Given the multiplet structure of figure 1A with $g_2 = 1$ and $M_2 = 5$, we have weights

$$\mathtt{w}_m = \begin{cases} \frac{1-\mathtt{w}}{4} & m < 4, \\ \mathtt{w} & m \geq 4. \end{cases} \tag{40}$$

The excitation energy correction is:

$$\left.\frac{\partial E^w_{\text{Hxc}}[\rho]}{\partial \mathtt{w}}\right|_{\rho=\rho^w} = -\frac{1}{4}\left(E_{\text{Hxc}}[\rho_{\text{GS}}] + E_{\text{Hxc}}[\rho_{\alpha\alpha}] + E_{\text{Hxc}}[\rho_{\beta\beta}] + E_{\text{Hxc}}[\rho_{\alpha\beta+\beta\alpha}]\right) + E_{\text{Hxc}}[\rho_{\alpha\beta-\beta\alpha}]. \tag{41}$$

As done for the bi-ensemble in section III A, we again enforce spin symmetry by using the energy $E_{\text{Hxc}}[\rho_{\alpha\alpha}]$ for all states in the triplet. The last term, representing the singlet, we write as $E_{\text{Hxc}}[\rho_{\alpha\beta\pm\beta\alpha}]$. The second excitation energy (i.e. the singlet), then is calculated as:

$$\Omega_2^{\text{e}} = \varepsilon_{n=2} - \varepsilon_{n=1} - \frac{1}{4}E_{\text{Hxc}}[\rho_{\text{GS}}] - \frac{3}{4}E_{\text{Hxc}}[\rho_{\alpha\alpha}] + E_{\text{Hxc}}[\rho_{\alpha\beta\pm\beta\alpha}]. \tag{42}$$

D. Tri-ensemble: Symmetry-broken

Using the symmetry-broken approach introduced in section III B, we simplify equation (41) using $E_{\text{Hxc}}[\rho_{\alpha\alpha}]$ for only two states in the triplet. $E_{\text{Hxc}}[\rho_{\alpha\beta\pm\beta\alpha}]$ is then used for the third state of the triplet and for the singlet state. The second excitation energy then is calculated as:

$$\Omega_2^{\text{b}} = \varepsilon_{n=2} - \varepsilon_{n=1} - \frac{1}{4}E_{\text{Hxc}}[\rho_{\text{GS}}] - \frac{1}{2}E_{\text{Hxc}}[\rho_{\alpha\alpha}] + \frac{3}{4}E_{\text{Hxc}}[\rho_{\alpha\beta\pm\beta\alpha}]. \tag{43}$$

(a) Symmetry-enforced tri-ensemble

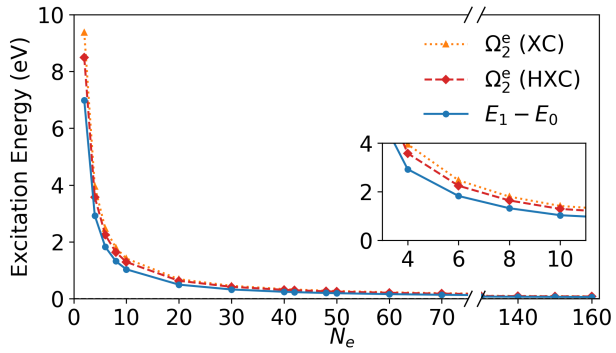

(b) Symmetry-broken tri-ensemble

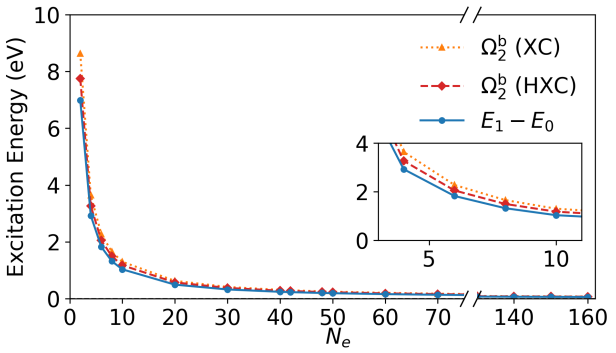

Figure 6. Energy of singlet states obtained as second excitation energies Ω_2 from the tri-ensemble compared to KS energy differences E_0–E_1 using **(a)** the symmetry-enforced tri-ensembles described in section III C and by equation (42), and **(b)** the symmetry-broken tri-ensemble described in section III D and by equation (43). Insets show detail of regions for small N_e. The labels 'e' and 'b' denote results from the symmetry-enforced and symmetry-broken ensembles. HXC denotes results with a weight-dependent Hartree, while XC denotes the use of a "traditional" Hartree, as explained in section II C.

Table I. Ensemble-corrected excitation energies tabulated versus number of electrons N_e, compared with KS energy difference $E_1 - E_0$, all reported in eV. Ω_1 and Ω_1^{flip} are the first excitation energies of the symmetry-enforced bi-ensemble (energy of triplet) and flipped symmetry-enforced bi-ensemble (energy of closed-shell singlet), respectively. Ω_2 are the second excitation energies, corresponding to the open-shell singlet, obtained from the symmetry-enforced and symmetry-broken tri-ensembles, respectively. The labels 'e' and 'b' denote results from the symmetry-enforced and symmetry-broken ensembles. HXC denotes results with a weight-dependent Hartree, while XC denotes the use of a "traditional" Hartree, as explained in section II C.

		Ω_1^e		Ω_1^b		$\Omega_1^{\text{flip,e}}$		$\Omega_1^{\text{flip,b}}$		Ω_2^e		Ω_2^b	
N_e	$E_1 - E_0$	XC	HXC	XC	HXC	XC	HXC	XC	HXC	XC	HXC	XC	HXC
2	6.988	0.2471	−10.29	3.190	−7.346	−4.741	−1.229	−5.722	−2.210	9.369	8.491	8.633	7.755
4	2.925	0.3339	−4.119	1.574	−2.879	−2.061	−0.5767	−2.474	−0.9901	3.949	3.578	3.639	3.268
6	1.822	0.2493	−2.454	1.027	−1.676	−1.298	−0.3970	−1.557	−0.6563	2.469	2.244	2.275	2.049
8	1.319	0.1687	−1.741	0.7424	−1.168	−0.9351	−0.2989	−1.127	−0.4902	1.797	1.638	1.653	1.494
10	1.032	0.1161	−1.350	0.5734	−0.8927	−0.7268	−0.2382	−0.8793	−0.3906	1.413	1.291	1.299	1.177
20	0.4931	0.0253	−0.6384	0.2558	−0.4079	−0.3372	−0.1159	−0.4140	−0.1928	0.6846	0.6293	0.6270	0.5717
30	0.3236	0.0065	−0.4189	0.1613	−0.2641	−0.2179	−0.0761	−0.2695	−0.1277	0.4520	0.4165	0.4133	0.3778
40	0.2408	0.0005	−0.3119	0.1172	−0.1952	−0.1607	−0.0566	−0.1996	−0.0954	0.3374	0.3114	0.3083	0.2822
42	0.2291	−0.0001	−0.2967	0.1111	−0.1855	−0.1527	−0.0538	−0.1897	−0.0909	0.3211	0.2964	0.2933	0.2686
48	0.1999	−0.0015	−0.2590	0.0960	−0.1615	−0.1327	−0.0469	−0.1652	−0.0794	0.2805	0.2591	0.2562	0.2347
50	0.1917	−0.0018	−0.2485	0.0918	−0.1548	−0.1153	−0.0165	−0.1584	−0.0762	0.3374	0.2486	0.2458	0.2252
60	0.1592	−0.0028	−0.2065	0.0754	−0.1283	−0.1052	−0.0373	−0.1313	−0.0634	0.2239	0.2069	0.2044	0.1874
70	0.1362	−0.0032	−0.1766	0.0640	−0.1095	−0.0897	−0.0319	−0.1121	−0.0543	0.1917	0.1772	0.1749	0.1605
80	0.1189	−0.0033	−0.1542	0.0555	−0.0956	−0.0782	−0.0279	−0.0978	−0.0475	0.1676	0.1550	0.1529	0.1403
90	0.1056	−0.0033	−0.1369	0.0490	−0.0846	−0.0693	−0.0248	−0.0867	−0.0422	0.1488	0.1377	0.1358	0.1246
100	0.0949	−0.0032	−0.1233	0.0439	−0.0762	−0.0622	−0.0222	−0.0779	−0.0379	0.1339	0.1239	0.1221	0.1121
110	0.0862	−0.0032	−0.1118	0.0397	−0.0689	−0.0564	−0.0202	−0.0707	−0.0345	0.1216	0.1126	0.1109	0.1019
120	0.0780	−0.0030	−0.1024	0.0363	−0.0631	−0.0516	−0.0185	−0.0647	−0.0316	0.1115	0.1031	0.1016	0.0933
130	0.0729	−0.0029	−0.0945	0.0334	−0.0582	−0.0476	−0.0171	−0.0597	−0.0292	0.1029	0.0952	0.0938	0.0862
140	0.0676	−0.0028	−0.0879	0.0309	−0.0541	−0.0441	−0.0158	−0.0554	−0.0270	0.0955	0.0884	0.0870	0.0800
150	0.0631	−0.0027	−0.0818	0.0288	−0.0503	−0.0412	−0.0148	−0.0517	−0.0253	0.0891	0.0825	0.0812	0.0746
160	0.0591	−0.0026	−0.0766	0.0269	−0.0471	−0.0385	−0.0139	−0.0484	−0.0237	0.0835	0.0773	0.0761	0.0699

The difference between excitation energies obtained from the symmetry-enforced and symmetry-broken tri-ensembles is

$$\Omega_2^e - \Omega_2^b = -\frac{1}{4}E_{xc}[\rho_{\alpha\alpha}] + \frac{1}{4}E_{xc}[\rho_{\alpha\beta\pm\beta\alpha}], \qquad (44)$$

which is simply $-1/4$ times the difference for the bi-ensemble.

IV. RESULTS AND DISCUSSION

A. Bi-ensembles and Triplet Instability

The corrected first excitation energies Ω_1^e from the bi-ensemble, according to the symmetry-enforced scheme, are shown in figure 5a. All numerical results are also tabulated in

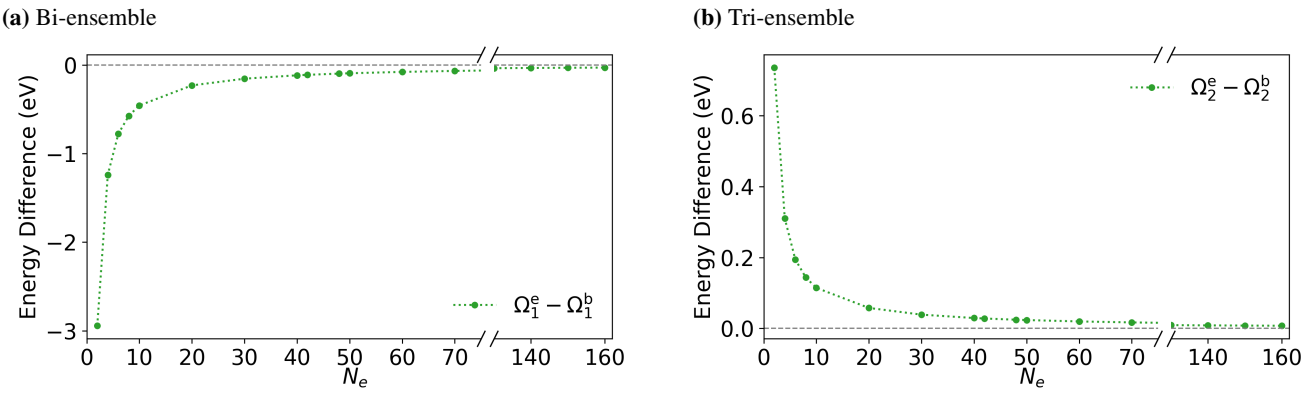

Figure 7. Difference between excitation energies of **(a)** triplet excited states from the symmetry-enforced (Ω_1^e) and symmetry-broken (Ω_1^b) bi-ensembles, as given in equation (39), **(b)** singlet excited states from the symmetry-enforced (Ω_2^e) and symmetry-broken (Ω_2^b) tri-ensembles, as given in equation (44). The labels 'e' and 'b' denote results from the symmetry-enforced and symmetry-broken ensembles.

table I. We find that in this case, like all cases we study in this paper, that the excitation energies go to zero in the thermodynamic limit, in agreement with the expectation from Luttinger liquid theory.[50] When a "traditional" Hartree DFA is used (the XC case), the ensemble-corrected triplet energies are positive for $N_e \leq 40$, after which they become negative, indicating that the triplet is lower in energy: a triplet instability. These XC excitation energies are one order of magnitude smaller than the KS difference in energies. With the ensemble-generalized LSDA HXC functional, Ω_1^e is negative for all N_e. The results from the symmetry-broken scheme are shown in figure 5b. There is an upward energy shift up to 3 eV compared to symmetry-enforced results, which makes the XC case positive for all N_e. The energy difference between symmetry-enforced and symmetry-broken is plotted in figure 7a. The HXC case remains negative for all N_e.

We note that finding a multiplet ordering different from the one assumed in construction of our ensemble means that the construction was invalid according to the rules of GOK EDFT, although this re-ordering is not a problem according to the more general EDFT definition in which weights must be monotonically non-increasing with energy only within a given symmetry.[60] Triplet instabilities are known to exist in other theories, such as Hartree-Fock,[65–67] time-dependent Hartree-Fock (TDHF),[68,69] and TDDFT.[70] Triplet instabilities have also been reported in the 3D electron gas at metallic densities.[71] In the 1D case, this instability appears to be a failure of the theory given the known singlet ground state.[48]

To investigate the triplet instability further, and attempt to correct our ensemble construction, we consider the possibility that the true system should have a triplet GS and a singlet first excited state, as suggested by the negative triplet excitation energy. The weighting scheme of this flipped system is:

$$\mathtt{w}_m = \begin{cases} \frac{1-\mathtt{w}}{3} & m < 3, \\ \mathtt{w} & m \geq 3. \end{cases} \tag{45}$$

This weighting provides an ensemble-corrected excitation energy from this triplet GS to the singlet:

$$\Omega_1^{\text{flip,e}} = E_0 - E_1 - E_{\text{Hxc}}[\rho_{\alpha\alpha}] + E_{\text{Hxc}}[\rho_{\text{GS}}], \tag{46}$$

where $E_0 - E_1 = \varepsilon_{n=1} - \varepsilon_{n=2}$. We use $E_{\text{Hxc}}[\rho_{\alpha\alpha}]$ for the energy of all states in the triplet, as for the symmetry-enforced bi-ensemble (section III A). For the symmetry-broken bi-ensemble, the flipped excitation energy is obtained from:

$$\Omega_1^{\text{flip,b}} = E_0 - E_1 - \frac{2}{3}E_{\text{Hxc}}[\rho_{\alpha\alpha}] - \frac{1}{3}E_{\text{Hxc}}[\rho_{\alpha\beta\pm\beta\alpha}] + E_{\text{Hxc}}[\rho_{\text{GS}}], \tag{47}$$

where we use $E_{\text{Hxc}}[\rho_{\alpha\alpha}]$ for the energy of just two in the triplet, and $E_{\text{Hxc}}[\rho_{\alpha\beta\pm\beta\alpha}]$ for the third, as was done for the symmetry-broken bi-ensemble (section III B). In both cases we treat $E_{\text{Hxc}}[\rho_{\text{GS}}]$ as the excited-state singlet. These results are shown in figure 5c-d. We find that the excitation energies are negative in all cases (XC and HXC, symmetry-enforced and symmetry-broken). The XC energy corrections are small, on the order of 0.01 eV in both the symmetry-enforced and symmetry-broken cases. An excitation energy in the flipped ensemble *opposite* to the original ensemble would provide a consistent picture of the energy ordering of the closed-shell singlet and the triplet. This is satisfied for the XC cases (except symmetry-enforced $N_e \geq 42$), which had not shown a triplet instability. However for HXC, though corrected energy differences are above the KS difference, the negative excitation energies contradict the instability of the triplet found in the original bi-ensembles. Thus the triplet instability for HXC is accompanied by an inconsistency about the energy ordering, indicating a deficiency of this approximation.

B. Singlet Excitations from Tri-ensembles

All singlet excitation energies from the tri-ensemble are positive (figure 6). For the symmetry-enforced tri-ensemble, the corrected second excitation energy Ω_2^e is greater in value than the KS second excitation energy E_1–E_0, regardless of whether a weight-dependent Hartree is used or not. The weight-dependent Hartree contribution is negative, and it is on the order of 0.01 eV lower than the XC correction at $N_e = 160$.

The symmetry-broken tri-ensemble provides a corrected second excitation energy Ω_2^b which is again greater in value

than the KS energy difference, whether the Hartree term used is weight-dependent or not. The corrections are somewhat smaller than in the symmetry-enforced case. The weight-dependent Hartree contribution is identical to the symmetry-enforced case, as discussed above. We find that the excitation energy difference between symmetry-enforced and symmetry-broken approaches is always positive and monotonically decreasing. It is about an order of magnitude smaller than the excitation energies themselves (figure 7), and around 25% of the correction, indicating that this distinction has only a moderate impact on the results (unlike for the bi-ensemble).

C. Effective Mass

Given that our excitation energies go to zero in the thermodynamic limit, we cannot meaningfully study corrections to the bandgap, but we instead investigate the effective mass to look for non-vanishing corrections. The effective mass is a useful parameter by which to validate a model's treatment of interactions, and it can be directly studied in real systems. For instance, many studies have tried to reproduce the experimentally measured occupied bandwidth of sodium, with varying success.[72–74] To compute an effective mass in our case, we consider the excitation as an energy difference between k-points k_2 and k_1 on parabolic bands in a UEG, as in equation (28). We assume that the k-points for the excitation are the same for the non-interacting system and the interacting, ensemble-corrected system, which is appropriate if the Fermi level is not shifted with respect to the states by the interaction, like the condition for a conserving approximation in many-body perturbation theory.[75] With these considerations, we obtain the effective mass as:

$$\frac{\Delta E^{\text{ip}}}{\Delta E^{\text{int}}} = \frac{E_I - E_0}{\Omega_I} = \frac{\frac{\hbar^2 {k_2}^2}{2m_e} - \frac{\hbar^2 {k_1}^2}{2m_e}}{\frac{\hbar^2 {k_2}^2}{2m^*} - \frac{\hbar^2 {k_1}^2}{2m^*}} = \frac{m^*}{m_e}. \tag{48}$$

While formally the effective mass is only defined for periodic systems, we study the behavior and limit of this ratio as our model approaches a periodic system. The effective masses at the thermodynamic limit (estimated as the results at our largest N_e, 160) are reported in Table II. In each case, the electron mass ratio approaches a limit which differs from the bare mass, in which case $m^*/m_e = 1$. By contrast, it can be shown analytically that GS DFT with LDA gives the effective mass in a UEG always equal to the free electron mass.[76] That a nontrivial change in the effective mass is found through EDFT shows the promise of EDFT for periodic systems, and the promise for additional insight to be obtained through the use of more sophisticated ensemble DFAs.

The effective masses for the bi-ensemble exhibit several different behaviors (figure 8). For the symmetry-enforced bi-ensemble with weight-dependent Hartree, the effective mass is negative and decreases monotonically until $N_e = 30$, after which point the effective mass increases slightly as it converges to its limit. The symmetry-broken bi-ensemble with weight-dependent Hartree also has a negative effective mass is negative which decreases monotonically throughout the range as it converges to its limit (except for a small bump at $N_e = 140$), to a more negative value that the symmetry-enforced case. These negative effective masses (related to the triplet instability in this case) indicate hole rather than electron character, which is unexpected for a metallic system. For the symmetry-enforced bi-ensemble with "traditional" Hartree, the effective mass is positive for small N_e, diverges near $N_e = 41$ and changes sign, reaching a negative limiting value. For the symmetry-broken bi-ensemble with "traditional" Hartree, the effective mass is positive for small N_e, decreases sharply to a minimum of 1.775 at $N_e = 6$, before increasing asymptotically towards its limit. The divergence appears pathological, although convergent limiting behavior is still achieved.

We find positive and monotonically decreasing effective masses in all cases for the tri-ensemble. The use of weight-dependent Hartree in the tri-ensemble results increases the effective mass by a fairly constant value of 0.06-0.09 in both version of the tri-ensemble, as shown in figures 8c-d. Construction of the flipped bi-ensemble leads to effective masses that are now positive, as expected. They show non-monotonic behavior and unexpectedly approach values substantially larger than 1, as shown in figure 9. The HXC results are systematically larger than for XC, and the symmetry-enforced results are systematically larger than the symmetry-broken results.

We are not aware of any reported values for the effective mass of electrons in the 1D UEG, so for comparison we will look at the literature for 2D and 3D UEGs. Conventionally, UEGs are characterized by the density parameter r_s, which is the Wigner-Seitz radius measured in Bohr radii a_0. The 1D generalization[63] is $r_s = a_0/2\rho$, which in our case is 1.89. We compare our results to the effective mass for the UEG obtained *via* Monte Carlo for 2D and 3D systems with $r_s \leq 4$, representing the metallic regime, where $r_s \leq 1$ represents the high-density regime.[77,78] In the 3D case, effective masses in the UEG obtained by variational diagrammatic Monte Carlo (MC) have been found to be 0.955(1) for $r_s = 1$, and 0.996(3) at $r_s = 4$.[77] Other calculations on the 3D UEG done via diffusion MC extrapolated to the thermodynamic limit have reported an effective mass of 0.85 at $r_s \approx 4$.[79] For a 2D UEG, diffusion MC gave results for a paramagnetic case of 0.955(2) at $r_s = 1$ and 1.04(2) at $r_s = 5$.[80] The ferromagnetic case gave 0.851(5) at $r_s = 1$ and 0.74(1) at $r_s = 5$;[80] one might imagine this would have some relation to the triplet instability, but the numerical values are very different from our results. In the high-density limit for a 3D electron gas, the effective mass is expected to be less than one.[81] Our 1D results in the range 0.7 to 0.85 from the tri-ensemble are fairly similar to the 2D and 3D cases. These results seem reasonable given the weak dependence on dimensionality seen between 2D and 3D, and the spread in literature values for the effective masses. The symmetry-enforced bi-ensemble with HXC gives -0.7714 which is similar in magnitude to the tri-ensemble results, but the other bi-ensemble cases seem increasingly unphysical with magnitudes up to -22.66.

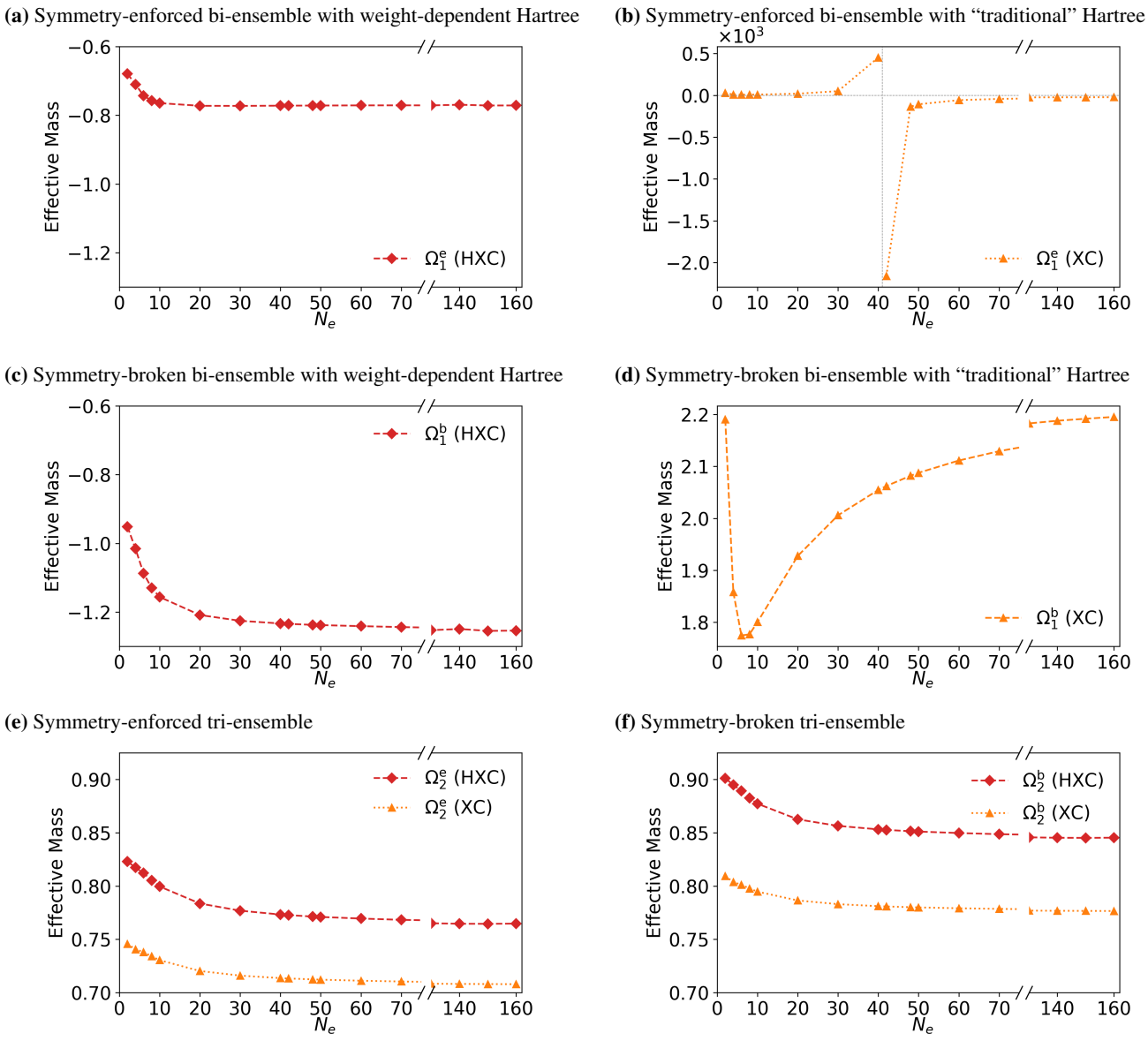

Figure 8. Effective masses, calculated from equation (48), for **(a, b)** the symmetry-enforced bi-ensemble described in section III A, **(c, d)** the symmetry-broken bi-ensemble described in section III B, **(e)** the symmetry-enforced tri-ensemble of section III C, and **(f)** the symmetry-broken tri-ensemble of section III D. In **(b)** a horizontal line is drawn at 0 and a vertical line marks the divergence around $N_e = 41$. The labels 'e' and 'b' denote results from the symmetry-enforced and symmetry-broken ensembles. HXC denotes results with a weight-dependent Hartree, while XC denotes the use of a "traditional" Hartree, as explained in section II C.

V. CONCLUSION

Since EDFT was designed for the treatment of discrete energy levels, it does not readily adapt to the band structure of solids. We have therefore instead approached the application of EDFT to a periodic system through a set of systems having the same fixed average density, and studied its approach to the thermodynamic limit. We have considered ensemble-corrected excitation energies for systems where the KS potential is set to the PIB potential, becoming the UEG in the thermodynamic limit, and avoiding the need for SCF calculations.

Corrections to the singlet energy obtained from a tri-ensemble are positive, increasing the KS energy differences. We find an apparently spurious triplet instability for bi-ensembles with weight-dependent Hartree, which is accompanied by inconsistency with the energy ordering from a bi-ensemble with flipped multiplets. In the symmetry-enforced bi-ensemble, with "traditional" Hartree, this instability is only found for $N_e > 40$, and no instability is found in the symmetry-broken bi-ensemble with "traditional" Hartree, yielding a corrected triplet energy which is higher than the KS energy. While EDFT provides nonzero corrections to excitation ener-

(a) Flipped symmetry-enforced bi-ensemble

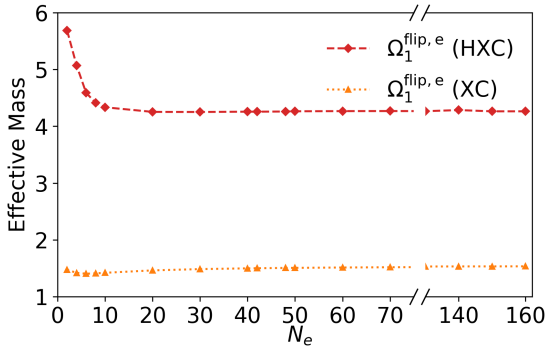

(b) Flipped symmetry-broken bi-ensemble

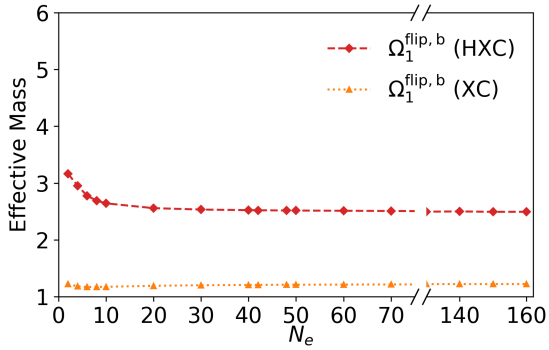

Figure 9. Effective mass, calculated from equation (48), for the flipped **(a)** symmetry-enforced and **(b)** symmetry-broken bi-ensemble described in section IV A. The labels 'e' and 'b' denote results from the symmetry-enforced and symmetry-broken ensembles. HXC denotes results with a weight-dependent Hartree, while XC denotes the use of a "traditional" Hartree, as explained in section II C.

Table II. Effective masses in the thermodynamic limit, estimated from $N_e = 160$, obtained from equation (48) using the ensemble-corrected excitation energies. The labels 'e' and 'b' denote results from the symmetry-enforced and symmetry-broken ensembles. HXC denotes results with a weight-dependent Hartree, while XC denotes the use of a "traditional" Hartree, as explained in section II C.

Excitation	HXC	XC
Ω_1^{e}	−0.7714	−22.66
Ω_1^{b}	−1.254	2.195
$\Omega_1^{\text{flip,e}}$	4.263	1.534
$\Omega_1^{\text{flip,b}}$	2.495	1.223
Ω_2^{e}	0.7648	0.7079
Ω_2^{b}	0.8454	0.7766

gies in the finite regime, in the approach to the thermodynamic limit, these tend to zero, as do the KS energy differences as well, which is expected for a metallic system.[47] We consider symmetry-enforced and symmetry-broken schemes of handling the triplet and singlet states that are indistinguishable in density, and find that for the bi-ensemble the symmetry-broken case leads to more physically reasonable results tha, whereas for the tri-ensemble the difference in results between the schemes is relatively small.

Effective masses for each of the methods were calculated, and found to approach a positive limit in the tri-ensemble, and a negative limit in most cases for the bi-ensemble. The flipped bi-ensemble led to positive values greater than 1. A non-trivial correction to the effective mass is found in the thermodynamic limit, even with our simple Hartree and LSDA XC approximations. Results in the range 0.7-0.85 are found from the tri-ensemble, similar to literature results for 2D and 3D UEGs. These results indicate the potential of EDFT in the periodic limit to provide meaningful results.

Prior work by Kraisler and Kronik[59] examined the derivative discontinuity of XC functionals (which corrects the KS gap) in the thermodynamic limit, based on ensemble considerations (but not on GOK EDFT). They note that the Hartree-based contribution to the missing derivative discontinuity vanishes in the thermodynamic limit, with the exact XC component being the source of a useful correction. They note that, as we see in our results, LDA-based corrections to the gap vanish due to known insufficiencies in this approximation. By contrast, our work, investigating effective masses as well, found that there can be a nontrivial correction from LDA in the thermodynamic limit.

We have investigated the impact of using two different forms of ensemble-generalized Hartree, one in which there is explicit weight dependence in the functional, which is then applied to densities of individual states, and one in which the weight-dependence is only accounted for in the ensemble density (the "traditional" Hartree). However, it is known that neither method treating the ensemble Hartree is sufficient to treat systems with "difficult" spin multiplets in finite systems.[43] The weight-dependent Hartree contribution has a minor impact for tri-ensembles, but for the bi-ensembles, we find its use leads to a triplet instability but more physically reasonable effective masses. In all cases we have used the former explicitly weight-dependent ensemble-generalized LDA XC. Given that neither LDA nor GGA in periodic systems exhibit the necessary divergence of f_{xc},[14] it reasonable to expect that implementation of more sophisticated ensemble DFAs, particularly non-local and GIE-free XC, would be needed for fuller analysis of EDFT's applicability and limitations in treating periodic systems.

While the treatment of increasingly large finite systems at a fixed average density may not be practical for extracting information about real systems, our results from this approach suggest that a formulation of EDFT for periodic systems could provide non-trivial results even with simple DFAs, and motivate further work on finding a suitable formulation. Further study of UEG systems in the thermodynamic limit can be extended to 2D and 3D, with a more realistic Coulomb interaction, as well as to models with a nonuniform potential, such as the Kronig-Penney model,[82] which is not metallic and can be used to investigate whether non-trivial bandgap corrections can be found. Finally, the study of systems with an odd num-

ber of electrons, which have a different multiplet structure, may offer further insight.

ACKNOWLEDGMENTS

R.J.L., D.A.S., and A.P.J. were supported by the U.S. Department of Energy, National Nuclear Security Administration, Minority Serving Institution Partnership Program, under Award DE-NA0003866. R.J.L. was also supported by the NRT program Convergence of Nano-engineered Devices for Environmental and Sustainable Applications (CONDESA) under NSF award DGE-2125510. Computational resources were provided by the Pinnacles cluster at Cyberinfrastructure and Research Technologies (CIRT), University of California, Merced, supported by the National Science Foundation Award OAC-2019144.

REFERENCES

[1] B. Senjean and E. Fromager, Phys. Rev. A **98**, 022513 (2018).
[2] J. P. Perdew and M. Levy, Phys. Rev. Lett. **51**, 1884 (1983).
[3] E. Runge and E. K. U. Gross, Phys. Rev. Lett. **52**, 997–1000 (1984).
[4] C. Ullrich, *Time-Dependent Density-Functional Theory: Concepts and Applications* (Oxford University Press, New York, 2011).
[5] M. A. L. Marques, N. T. Maitra, F. Nogueira, E. K. U. Gross, and A. Rubio, *Fundamentals of Time-Dependent Density Functional Theory*, Lecture Notes in Physics, Vol. 837 (Springer, Heidelberg, Germany, 2012).
[6] E. R. Davidson and L. Z. Stenkamp, Int. J. Quantum Chem. **10**, 21–31 (1976).
[7] R. McWeeny, Mol. Phys. **28**, 1273–1282 (1974).
[8] P. C. De Mello, M. Hehenberger, and M. C. Zernert, Int. J. Quantum Chem. **21**, 251–258 (1982).
[9] D. Jacquemin, E. A. Perpète, I. Ciofini, C. Adamo, R. Valero, Y. Zhao, and D. G. Truhlar, J. Chem. Theory Comput. **6**, 2071–2085 (2010).
[10] M. E. Casida, "Time-dependent density functional response theory of molecular systems: Theory, computational methods, and functionals," in *Recent Developments and Applications of Modern Density Functional Theory*, Theoretical and Computational Chemistry, Vol. 4 (Elsevier Science BV, Amsterdam, 1996) Chap. 11, pp. 391–434.
[11] M. Huix-Rotllant, A. Ipatov, A. Rubio, and M. E. Casida, Chem. Phys. **391**, 120–129 (2011).
[12] P. Elliott, S. Goldson, C. Canahui, and N. T. Maitra, Chem. Phys. **391**, 110–119 (2011).
[13] N. T. Maitra, Annu. Rev. Phys. Chem. **73**, 117–140 (2022).
[14] G. Onida, L. Reining, and A. Rubio, Rev. Mod. Phys. **74**, 601–659 (2002).
[15] C. A. Ullrich and Z. Yang, Braz. J. Phys. **44**, 154–188 (2014).
[16] N. T. Maitra, F. Zhang, R. J. Cave, and K. Burke, J. Chem. Phys. **120**, 5932–5937 (2004).
[17] A. Dreuw, J. L. Weisman, and M. Head-Gordon, J. Chem. Phys. **119**, 2943–2946 (2003).
[18] S. Botti, A. Schindlmayr, R. D. Sole, and L. Reining, Rep. Prog. Phys. **70**, 357 (2007).
[19] L. J. Sham and M. Schlüter, Phys. Rev. Lett. **51**, 1888–1891 (1983).
[20] R. W. Godby and I. D. White, Phys. Rev. Lett. **80**, 3161–3161 (1998).
[21] M. K. Y. Chan and G. Ceder, Phys. Rev. Lett. **105**, 196403 (2010).
[22] E. K. U. Gross, L. N. Oliveira, and W. Kohn, Phys. Rev. A **37**, 2809 (1988).
[23] E. K. U. Gross, L. N. Oliveira, and W. Kohn, Phys. Rev. A **37**, 2805 (1988).
[24] F. Sagredo and K. Burke, J. Chem. Phys. **149**, 134103 (2018).
[25] K. Deur, L. Mazouin, and E. Fromager, Phys. Rev. B. **95**, 035120 (2017).
[26] E. Kraisler and L. Kronik, Phys. Rev. Lett. **110**, 126403 (2013).
[27] J. P. Perdew, R. G. Parr, M. Levy, and J. L. Balduz Jr., Phys. Rev. Lett. **49**, 1691–1694 (1982).
[28] Z. Yang, J. R. Trail, A. Pribram-Jones, K. Burke, R. J. Needs, and C. A. Ullrich, Phys. Rev. A **90**, 042501 (2014).
[29] Z. Yang, A. Pribram-Jones, K. Burke, and C. A. Ullrich, Phys. Rev. Lett. **119**, 033003 (2017).
[30] A. Borgoo, A. M. Teale, and T. Helgaker, AIP Conf. Proc. **1702**, 090049 (2015).
[31] A. Pribram-Jones, Z. Yang, J. R. Trail, K. Burke, R. J. Needs, and C. A. Ullrich, J. Chem. Phys. **140**, 18A541 (2014).
[32] K. Deur, L. Mazouin, B. Senjean, and E. Fromager, Eur. Phys. J. B **91**, 162 (2018).
[33] K. Deur and E. Fromager, J. Chem. Phys **150**, 094106 (2019).
[34] M. Filatov, WIREs Comput. Mol. Sci. **5**, 146–167 (2015).
[35] T. Gould, Z. Hashimi, L. Kronik, and S. G. Dale, J. Phys. Chem. Lett. **13**, 2452–2458 (2022).
[36] E. K. U. Gross, L. N. Oliveira, and W. Kohn, Phys. Rev. A **37**, 2821 (1988).
[37] W. Kohn, Phys. Rev. A **34**, 737–741 (1986).
[38] Á. Nagy, Int. J. Quantum Chem. **69**, 247–254 (1998).
[39] N. I. Gidopoulos, P. G. Papaconstantinou, and E. K. U. Gross, Phys. Rev. Lett. **88**, 033003 (2002).
[40] Á. Nagy, Int. J. Quantum Chem. **56**, 297–301 (1995).
[41] C. Marut, B. Senjean, E. Fromager, and P.-F. Loos, Faraday Discuss. **224**, 402 (2020).
[42] Z. Yang, Phys. Rev. A **104**, 052806 (2021).
[43] T. Gould, G. Stefanucci, and S. Pittalis, Phys. Rev. Lett. **125**, 233001 (2020).
[44] T. Gould and S. Pittalis, Phys. Rev. Lett. **123**, 016401 (2019).
[45] X. Andrade, D. A. Strubbe, U. De Giovannini, A. H. Larsen, M. J. T. Oliveira, J. Alberdi-Rodriguez, A. Varas, I. Theophilou, N. Helbig, M. J. Verstraete, L. Stella, F. Nogueira, A. Aspuru-Guzik, A. Castro, M. A. L. Marques, and A. Rubio, Phys. Chem. Chem. Phys. **17**, 31371–31396 (2015).
[46] N. Tancogne-Dejean, M. J. T. Oliveira, X. Andrade, H. Appel, C. H. Borca, G. Le Breton, F. Buchholz, A. Castro, S. Corni, A. A. Correa, U. De Giovannini, A. Delgado, F. G. Eich, J. Flick, G. Gil, A. Gomez, N. Helbig, H. Hübener, R. Jestädt, J. Jornet-Somoza, A. H. Larsen, I. V. Lebedeva, M. Lüders, M. A. L. Marques, S. T. Ohlmann, S. Pipolo, M. Rampp, C. A. Rozzi, D. A. Strubbe, S. A. Sato, C. Schäfer, I. Theophilou, A. Welden, and A. Rubio, J. Chem. Phys. **152**, 124119 (2020).
[47] E. Kaxiras and J. D. Joannopoulos, *Quantum Theory of Materials*, 1st ed. (Cambridge University Press, New York, 2019).
[48] E. Lieb and D. Mattis, Phys. Rev. **125**, 164–172 (1962).
[49] A. Malatesta and G. Senatore, J. Phys. IV France **10**, Pr5–341–Pr5–346 (2000).
[50] F. D. M. Haldane, J. Phys. C: Solid State Phys. **14**, 2585 (1981).
[51] A. Imambekov, T. L. Schmidt, and L. I. Glazman, Rev. Mod. Phys. **84**, 1253–1306 (2012).
[52] T. A. Wesolowski and A. Savin, "Non-additive kinetic energy and potential in analytically solvable systems and their approximated counterparts," in *Recent progress in orbital-free density functional theory*, edited by T. A. Wesolowski and Y. A. Wang (World Scientific, 2013) pp. 275–295.
[53] A. Szabo and N. S. Ostlund, *Modern Quantum Chemistry*, Dover Books on Chemistry (Dover Publications, Newburyport, 2013).
[54] A. K. Theophilou and N. I. Gidopoulos, Int. J. Quantum Chem. **56**, 333–336 (1995).
[55] N. D. Mermin, Phys. Rev. **137**, A1441–A1443 (1965).
[56] N. Marzari, D. Vanderbilt, and M. C. Payne, Phys. Rev. Lett. **79**, 1337–1340 (1997).
[57] T. Gould and S. Pittalis, Phys. Rev. Lett. **119**, 243001 (2017).
[58] E. Pastorczak and K. Pernal, J. Chem. Phys. **140**, 18A514 (2014).
[59] E. Kraisler and L. Kronik, J. Chem. Phys. **140**, 18A540 (2014).
[60] T. Gould and S. Pittalis, Aust. J. Chem. **73**, 714–723 (2020).
[61] J. J. Sakurai and J. Napolitano, *Modern Quantum Mechanics*, 3rd ed. (Cambridge University Press, New York, 2020).
[62] N. Helbig, J. I. Fuks, M. Casula, M. J. Verstraete, M. A. L. Marques, I. V. Tokatly, and A. Rubio, Phys. Rev. A **83**, 032503 (2011).
[63] M. Casula, S. Sorella, and G. Senatore, Phys. Rev. B **74**, 245427 (2006).
[64] S. Lehtola, C. Steigemann, M. J. T. Oliveira, and M. A. L. Marques, SoftwareX **7**, 1–5 (2018).
[65] A. W. Overhauser, Phys. Rev. Lett. **4**, 415–418 (1960).
[66] K. Sawada and N. Fukuda, Prog. Theor. Phys. **25**, 653–666 (1961).
[67] R. Lefebvre and Y. G. Smeyers, Int. J. Quantum Chem. **1**, 403–419 (1967).
[68] A. Dreuw and M. Head-Gordon, Chem. Rev. **105**, 4009–4037 (2005).

[69] J. Čížek and J. Paldus, J. Chem. Phys. **47**, 3976–3985 (2004).
[70] M. J. G. Peach and D. J. Tozer, J. Phys. Chem. A **116**, 9783–9789 (2012).
[71] J. Lam, Phys. Rev. B **3**, 1910–1918 (1971).
[72] R. Maezono, M. D. Towler, Y. Lee, and R. J. Needs, Phys. Rev. B **68**, 165103 (2003).
[73] A. Puente, L. Serra, and M. Casas, Z. Phys. D - Atoms Molec. Clusters **31**, 283–286 (1994).
[74] C. Fiolhais, F. Nogueira, and M. A. L. Marques, *A Primer in Density Functional Theory*, 1st ed., Lecture Notes in Physics, 620 (Springer, Berlin, 2003).
[75] G. Baym and L. P. Kadanoff, Phys. Rev. **124**, 287–299 (1961).
[76] S. G. Louie, "Predicting materials and properties: Theory of the ground and excited state," in *Conceptual Foundations of Materials*, Contemporary Concepts of Condensed Matter Science, Vol. 2, edited by S. G. Louie and M. L. Cohen (Elsevier, Amsterdam, 2006) Chap. 2, pp. 9–53.
[77] K. Haule and K. Chen, Sci. Rep. **12**, 2294 (2022).
[78] R. G. Parr and W. Yang, *Density-Functional Theory of Atoms and Molecules*, The International Series of Monographs on Chemistry (Oxford University Press, New York, 1989).
[79] S. Azadi, N. D. Drummond, and W. M. C. Foulkes, Phys. Rev. Lett. **127**, 086401 (2021).
[80] N. D. Drummond and R. J. Needs, Phys. Rev. B **87**, 045131 (2013).
[81] A. Krakovsky and J. K. Percus, Phys. Rev. B **53**, 7352–7356 (1996).
[82] R. d. L. Kronig and W. G. Penney, Proc. R. Soc. Lond. A **130**, 499–513 (1931).